Short fatigue crack growth behavior in 18Ni marageing steel

Z.K. Xu [a, b], B. Wang [a], P. Zhang [a, b*] and Z.F. Zhang [a, b*]

[a] *Shi-changxu Innovation Center for Advanced Materials, Institute of Metal Research, Chinese Academy of Sciences, Shenyang 110016, China*

[b] *School of Materials Science and Engineering, University of Science and Technology of China, Hefei 230026, China*

Abstract

In recent decades, it has been found that the fatigue crack growth rate could be slowed down by the zigzag crack growth path in some materials, but the mechanism was not well clarified. In this study, the effect of crack growth path on the fatigue crack growth rate of 18Ni maraging steel under three different heat treatment states was studied, and two factors influencing the fatigue crack growth rate were outlined. It was found that, firstly, the main factor affecting the fatigue crack growth rate was the strength of the material; secondly, the zigzag crack growth path did not slow down the crack growth rate but increased the crack growth rate. Therefore, a two-phase model was established to understand the influence of crack growth path on the growth rate. In different phases, their resistances to the crack growth are different, and the difference in the strength between the two phases determines whether the zigzag cracking path can depress the fatigue crack growth or not. Specifically, when the difference in the strength between the second phase and the matrix is greater than a certain value, the zigzag cracking path leads to the acceleration of fatigue crack growth. The consequences show that not all the zigzag crack propagation paths are beneficial for the higher fatigue cracking resistance, and the specific analysis should be combined with the material microstructure in detail.

Keywords: Maraging steel; Strength; Short crack; Fatigue crack propagation; Zigzag path; Lath martensite.

* Corresponding authors.
E-mail addresses: pengzhang@imr.ac.cn (P. Zhang), zhfzhang@imr.ac.cn (Z.F. Zhang).

1. Introduction

Maraging steels have been widely used in the most challenging structural application due to their ultra-high strength, high toughness and simple heat treatment [1-3]. For example, they were used in rocket engines, missile shells, aircraft landing gear, high-pressure vessels, and high-strength gear [4-7]. In such applications, the components often bear with cyclic loading, so that they are likely to fail at low-stress levels during the service and cause catastrophic consequences. Therefore, for the safety-critical structure, it is necessary to assume and consider the presence of defects like a short crack below a certain size [8]. In general, the crack propagation life is a combination of two parts: the short crack propagation life and the long crack propagation life. The long crack propagation life is short compared to the short crack propagation life [8]. Therefore, it is necessary to make a specialty of the study for short fatigue crack growth (FCG) and develop methods to reduce the short FCG rate.

Recently, it has been reported that the zigzag propagation paths could reduce the FCG rate [9-13]. The explanations can be summarized as the enhanced roughness-induced crack closure, the stress redistribution, and the reduction in crack tip opening distance (CTOD) because of the opening of sub-cracks [10]. All of the above explanations are about the advantages of the zigzag path. However, there may raise a scientific question: does the zigzag path have negative effects on the crack growth rate?

To answer that question, it needs to learn about why there would be a zigzag path in a fatigue crack growth path. In general, the zigzag path can be divided into two types in terms of its scale. Firstly, in the grain scale, it could be the intergranular or intragranular crack such as the cracks propagate along the grain boundary in ultrafine-grained materials [11] or the crack paths are parallel to one of the slip systems with a high Schmidt factor in each grain [12]. Secondly, the cracks may deflect within the grain. For instance, Ju *et al.* reported that a high-Mn austenitic alloy exhibited fatigue-crack growth along the $\{111\}_{\gamma}$ plane in addition to conventional mode I propagation [10]. Wang *et al.* reported that the crack path deflects because of the orderly distributed laths in a titanium alloy [13].

It is worth noted that the grain boundary of the fine-grain material, the slip surface with high Schmidt factor, the $\{111\}_\gamma$ slip plane in austenite, and the lath boundary (LB) in titanium alloy can be considered as the soft domain in strength. Thus, a hypothesis is raised that the crack deflects because there is a soft domain deviated from the original crack direction and the crack turns to the direction of the soft domain. In other words, the crack deviates to the soft domain with a lower FCG resistance and so it should accelerate the FCG rate [11]. So here is the conflict: whether does the zigzag path accelerate or decrease the FCG rate? Besides, the decreasing crack growth rates due to the zigzag path were mostly reported in the long crack; how about the short FCG?

To explore these problems, we selected three ageing-treatment conditions in 18Ni maraging steel with the microstructure of lath martensite to reveal the relationship between the zigzag path and the short FCG rate. The short FCG rate test was performed and the crack growth morphologies were carefully observed. The experimental results are discussed with a focus on the mechanisms of the accelerating growth and the role of the LB cracking.

2. Experimental

2.1. Materials

The material used in the present study was 18Ni maraging steel with elemental composition as seen in Table 1. The bars were quenched in water after heated at 850 ℃ for one hour, followed by three different ageing treatments, which were 500 ℃ for 5 h, 550 ℃ for 5 h, and 630 ℃ for 3 h. Electro-etching was used to reveal the microstructures and the compositions of the etchant were 10% HClO4 and 90% alcohol. A direct-current power supply was used and the voltage was 21.5 V. The specimens were etched for 50 seconds in the etchant, which was cooled by the ice water. The microstructure pictures were taken by LEO SUPRA 35 scanning electron microscopes (SEM) using the Inlens channel. The electron gun voltage was 20 kV and the working distance was 12 mm. The tensile test, using specimens with a gauge section 15×1.5×1 mm^3, was carried out on the Instron 5982 testing machine at room temperature and the

strain rate was 0.9 mm/min. Three specimens were tested for each ageing treatment.

Table 1. Elemental compositions of the experimental maraging steel (wt.%).

Ti	Cr	Mo	Ni	Si	Mn	P	S	C	Fe
1.55	0.21	3.24	18.4	0.07	<0.005	<0.005	<0.003	<0.02	Bal.

2.2. Short crack preparation

The preparation of through-thickness short crack consisted of several steps. Firstly, the pre-cracking of three-point bending specimens (as shown in Fig. 1a) was carried out on the Instron 8801 testing machine with a frequency of 20 Hz and the stress ratio of $R = 0.1$. The *K*-decreasing method was employed for the pre-cracking to save time and obtain a crack with a small tip plastic zone. The 20% reduction was adopted and the final K_{max} was about 7.5 MPa·m$^{1/2}$. Secondly, the three-point bending specimens were cut into four pieces along the trajectory as shown in Fig. 1b by electrical discharge machining (EDM). It was reported that there would be residual compressive stress in the specimen surfaces in high-strength steels [14]. To avoid the surface residual stress, 1 mm blank on each side of the 16 mm wide three-point bending specimen was removed by EDM as shown in Fig. 1b. The most part of the pre-crack was removed by the machining (as shown in Fig. 1c). Thirdly, the specimen surfaces were ground by SiC papers with 3000 grit size. Then, the crack depth in both sides of the specimen was measured using OLYMPUS GX71 optical microscope with shift light mode. After that, a target width of specimens was set by subtracting the length needed to be ground from the original width. The specimen surface containing the crack (as shown in Fig. 1d) was carefully ground by SiC papers from 400 to 3000 grit size. Fourthly, when the target width was reached, the specimens were cut into the same width by electrical discharge machining from the opposite. Note that the geometry of the specimen was designed for conveniently grinding so that an automatic polishing machine can be used. The final configuration of the fatigue specimen can be seen in Fig. 1e.

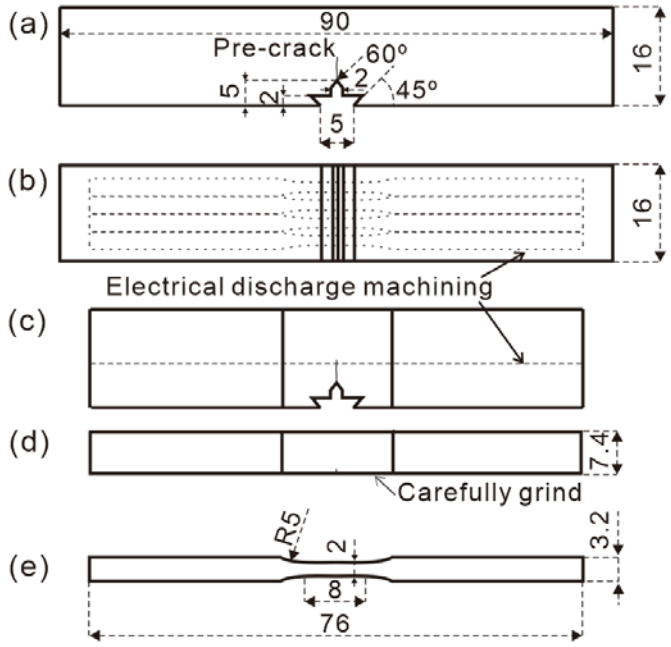

Fig. 1. The procedures of the specimen preparation. (a) Configuration of the three-point bend specimens. (b) and (c) The electrical discharge machining trajectory marked by the dotted line. (d) The surface needed to be carefully ground to obtain a short crack. (e) Configuration of specimens bearing pull-push load.

2.3. Short fatigue crack growth rate test

The fatigue life test of the specimen containing a short crack was carried out on the Instron 8801 testing machine with a frequency of 30 Hz and stress radio of $R = -1$. The environment temperature was about 20 ℃ and relative humidity was about 40%. The fracture surfaces were observed by a Keyence VHX-1000 digital stereoscopic microscope for color information. On each fracture surface, ten crack lengths were measured evenly along the thickness direction and the crack length was represented by the mean value. The error bar was represented by the standard error.

3. Results

3.1. Microstructures and tensile property

The microstructure predominantly consists of lath martensite [7, 15]. Due to the different reaction rates of the substructure in electropolishing, the substructure could be recognized clearly from Fig. 2. The substructure of martensite can be further described

as lath and LB, and the precipitates are mainly encompassed in the lath as shown in Fig. 2. It has been reported that the microstructure of LB is the reverted austenite caused by the micro-segregation of Ni, which is austenite stabilizing solute, along the boundary [15-17]. As the ageing temperature increases, the LB coarsens gradually, the precipitates grow up gradually, and the yield strength decreases as shown in Table 2. Since the growing up of the precipitates may lead to an increase of precipitate spacing, the yield strength decreases according to the Orowan strengthening mechanism. Previous researches had reported that the precipitates were mainly Ni_3(Ti, Mo) [7, 18, 19] and the effect of the microstructure evolution on the tensile properties is consistent with the results reported by Li *et al.* [18-22].

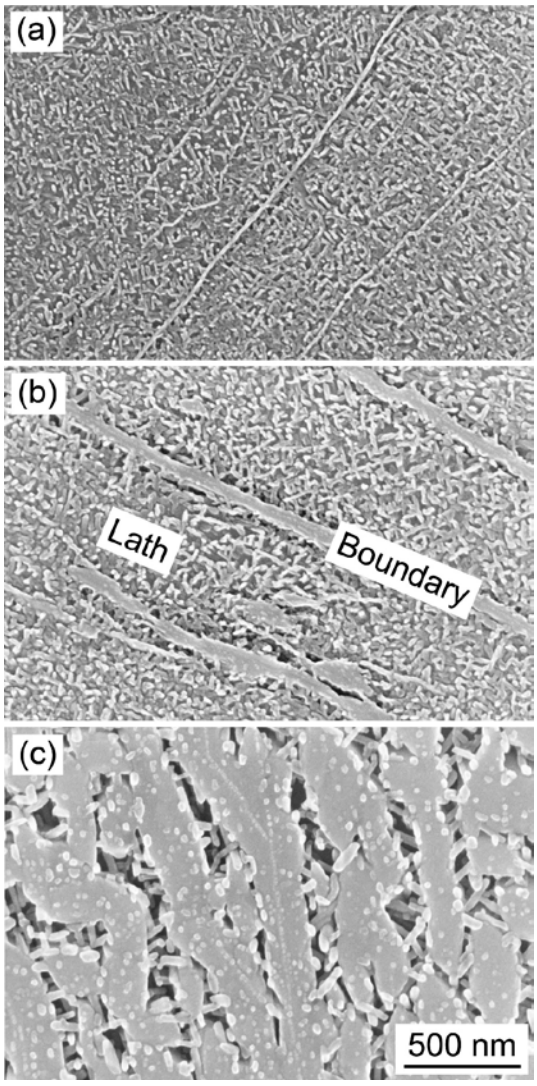

Fig. 2. The microstructure of the materials under ageing treatment of (a) 500 ℃ for 5 h, (b) 550 ℃ for 5 h and (c) 630 ℃ for 3 h. All the images share the same scale.

Table 2. Tensile properties of specimens under different ageing treatments.

Ageing treatment conditions	Material Label	Yield strength, σ_{YS} (MPa)	Ultimate tensile strength, σ_{UTS} (MPa)
500 ℃ for 5 h	500	1935 ± 22	1967 ± 17
550 ℃ for 5 h	550	1722 ± 25	1777 ± 23
630 ℃ for 3 h	630	944 ± 9	1335 ± 13

3.2. Short fatigue crack growth behavior

The measurement of the short FCG rate is not as easy as the long crack. The crack is too small to use the crack opening distance gauge employed in the flexibility method which is commonly used for the long crack. Normally, the length of the short fatigue crack was directly measured from the surface [23]. However, the crack length measured through the above method is not the real crack length. Another way is the nondestructive measurement such as the three-dimension X-ray diffraction topography (XRT) [24]. Unfortunately, because the opening distance of the short fatigue crack tip is extremely small, it is beyond the resolution of the XRT. Nevertheless, the real crack length is necessary for the present study, so the multiple sample method is employed.

The pre-crack zone can be clearly recognized from the fracture surfaces as shown in Fig. 3, which illustrates different crack lengths from ~50 μm to ~800 μm. From the view of pictures in Fig. 3, one conclusion can be drawn that all of the fracture surfaces are similar on the whole except for the difference of initial crack length. As the initial crack length increases, the cycles to failure decrease, as seen in Fig. 4. For the specimens at different ageing treatments, the specimen aged at 630 ℃ for 3 h has the lowest fatigue life during the whole span of initial crack length. The reason for that may be that the specimens aged at 630 ℃ for 3 h has the lowest yield strength, and the yield strength of material is a key factor influencing the short FCG rate. However, the specimens under ageing treatments of 500 ℃ for 5 h and 550 ℃ for 5 h seem to have rarely been affected by the ageing treatment, because their data appear to overlap as shown in Fig. 4.

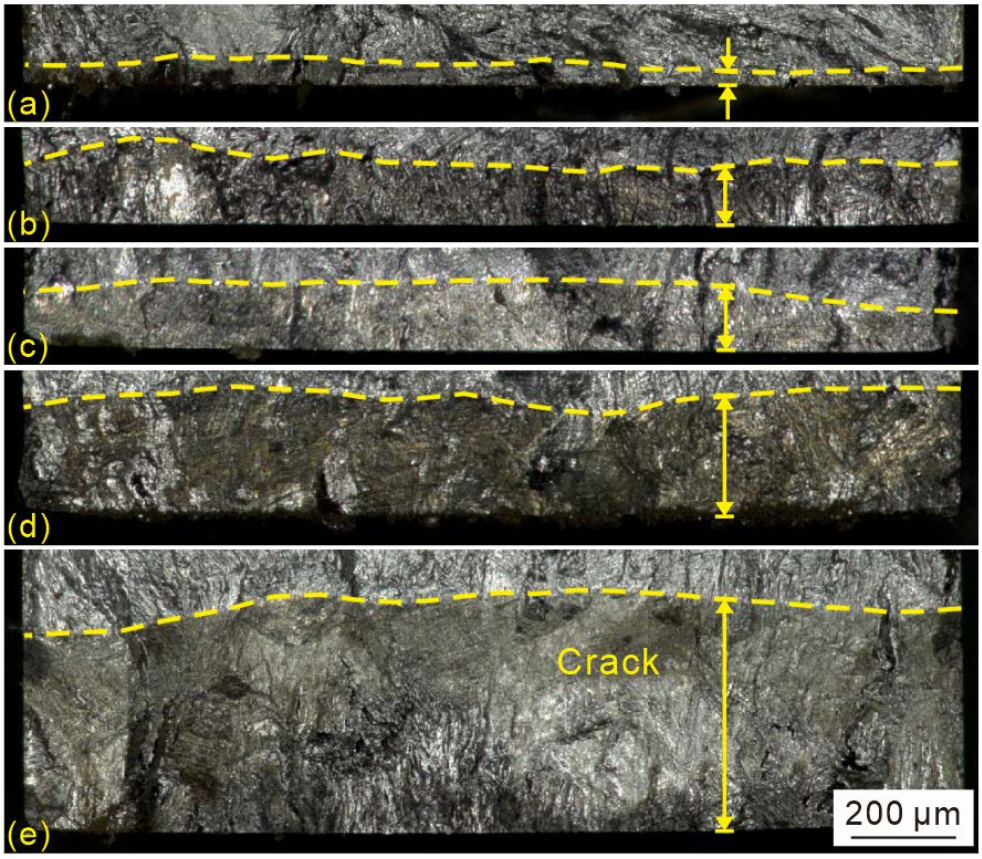

Fig. 3. Measurement of initial crack length through the picture taken by optical microscopy. The front of the crack is marked by the dotted line; (a) 57 ± 25 μm. (b) 156 ± 24 μm. (c) 160 ± 23 μm. (d) 310 ± 19 μm. (e) 769 ± 44 μm.

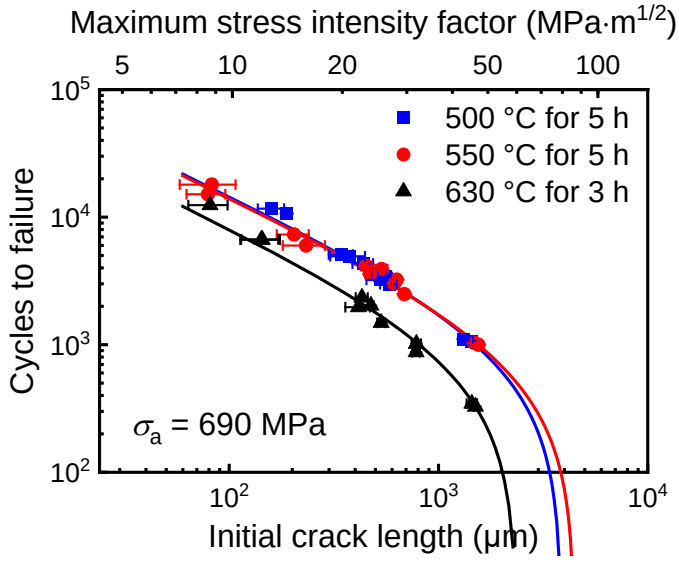

Fig. 4. Relationship between initial crack length and cycles to failure for specimens under different ageing treatments fatigued at constant stress amplitude of 690 MPa.

To clearly represent the short FCG behavior of the specimens under different

ageing treatments, the Paris law is employed:

$$\frac{\mathrm{d}a}{\mathrm{d}N} = C(\Delta K)^m , \tag{1}$$

where C and m are constants of material, ΔK is the stress intensity factor range. By the mathematical operation of integration, the residual life for a specimen containing an initial crack length of a_0 could be estimated as below:

$$N_\mathrm{p} = \frac{a_0^{(1-m/2)} - a_{\max}^{(1-m/2)}}{C\sigma_\mathrm{a}^m Y^m \pi^{m/2}(m/2-1)} + N_{\mathrm{p}|a_0=a_{\max}} , \tag{2}$$

where $a_{\max}$ is the longest initial crack, $N_{\mathrm{p}|a_0=a_{\max}}$ is the residual life cycles of the specimen containing the crack length corresponding to $a_{\max}$, σ_a is the stress amplitude of the fatigue loading, Y is the crack shape factor. By fitting the data listed in Fig. 4 with Eq. (2), the coefficient C in Paris law could be obtained as shown in Table 3. The results could be summarized in two aspects. First, it is evident that the exponent m in Paris law is almost the same for the specimens under different ageing treatments. Second, in the view of the coefficient C in Paris law, material 630 has the fastest FCG rate, while somehow, the materials 500 and 550 have the same performance in FCG rate.

Table 3. Coefficients of fatigue crack growth rate curve in the form of Paris law.

Material No.	C (mm/cycle)	m
500	1.1×10^{-10}	3.53
550	1.1×10^{-10}	3.54
630	2.0×10^{-10}	3.52

3.3. Crack morphology

To better recognize the behavior of short FCG of materials under different ageing treatments, the crack growth paths were carefully observed. Fig. 5 shows two different angles of martensite lath and fatigue loading for every ageing treatment, which are about 0° and 45°, respectively. For those about 0°, it is evident that material 500 has LB branch cracks along the primary crack, while materials 550 and 630 are not. For

those 45°, the crack path in material 500 is made by two parts: the inter-lath crack and the intra-lath crack (their angle is about 90º). Except for the main crack, there are some sub-cracks in the LB for material 500. As for material 550, the crack path is relatively smooth and does not have the 90º deflection like the path in material 500. As for material 630, the crack morphology is very similar to the titanium alloy [13]. It is explained that the lath is not strong enough to completely deflect the fatigue crack path [13]. Due to the LB cracking in material 500, more orientations were observed as shown in Fig 6. It can be seen that the morphologies of about 15º and 30º (as shown in Figs. 6a and b) are similar to that of about 0º (as shown in Fig. 5a). As for the morphologies of about 60º, there is a clear subcrack parallel to the primary crack. Instead of connecting to the main crack, it formed beside the main crack. It is similar to the result of high-Mn austenitic alloys and its microstructure is austenite/martensite lath [10].

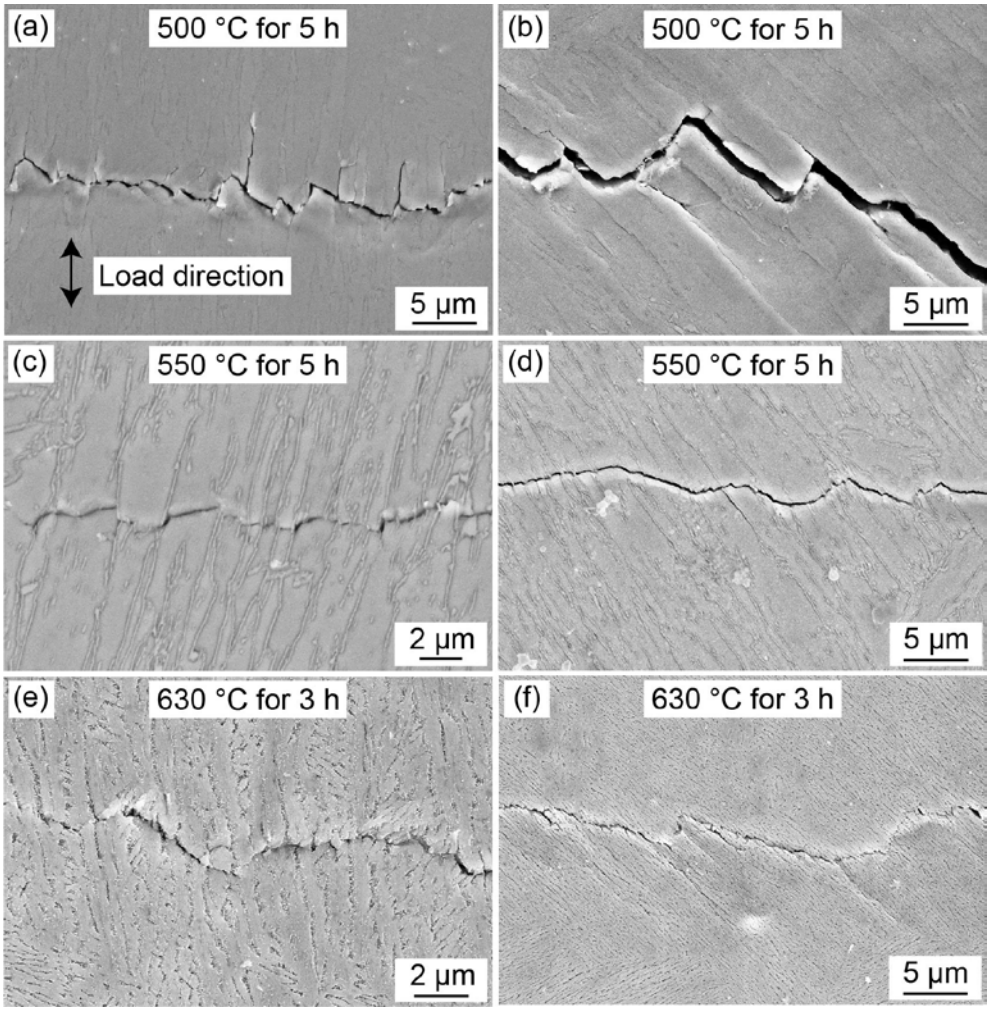

Fig. 5. Fatigue crack damage morphologies when the angle between martensite lath and

loading direction is about 0° ((a), (c) and (e)) and 45° ((b), (d) and (e)). The crack grows from left to right.

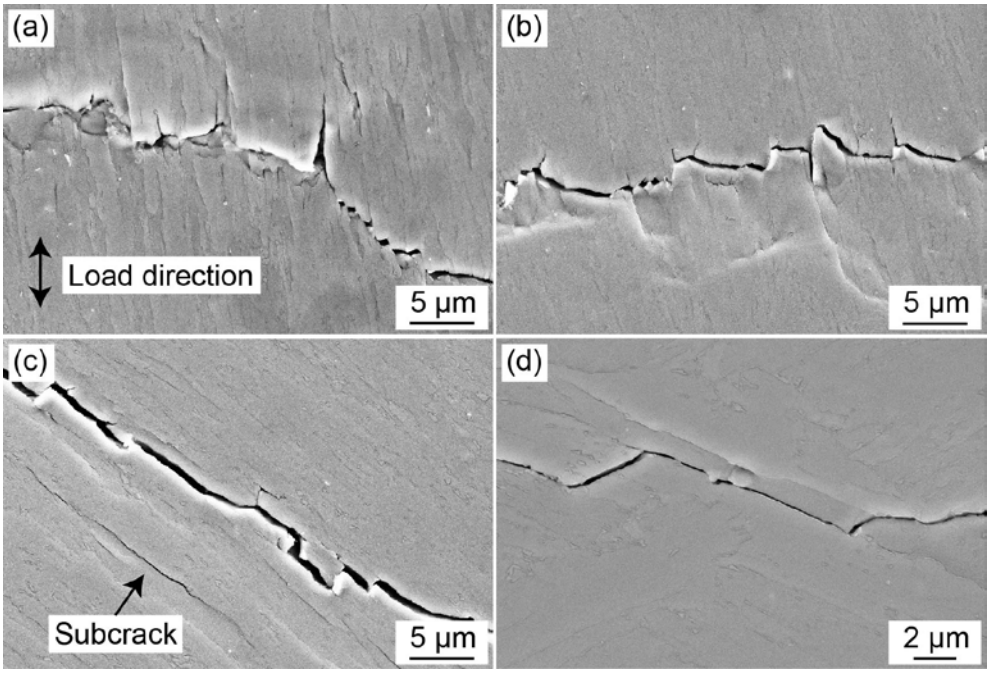

Fig. 6. Fatigue crack damage morphologies for material 500 when the angle between martensite lath and loading direction is about (a) 15°, (b) 30°, (c) 60° and (d) 75°. Crack grows from left to right.

In summary, it is found that material 630 has the lowest yield strength, but the fastest FCG rate. However, the gap between the FCG rate of materials 500 and 550 can be rarely seen although they have a quite different yield strength. In the view of crack morphologies, the LB cracking is found in material 500, while the LB stays uncracked in materials 550 and 630. Therefore, the relationships between the FCG rate and the yield strength and the crack morphology are needed to be discussed.

4. Discussion

4.1. The relation between fatigue crack growth rate and yield strength

Based on the experimental results above, several features for short FCG in specimens under different ageing treatments could be outlined. Firstly, the values of Paris exponent m in Eq. (1) for all three materials are nearly the same. That is to say, the FCG rate is mainly determined by the value of Paris coefficient C in Eq. (1).

Secondly, for materials 550 and 630, their crack morphologies have the same type that the LB stays uncracked, which means that the FCG rate represents the real crack resistance of the material. It is worth noting that the crack morphologies still have the same type for materials 550 and 630, while the FCG rate of material 630 is higher than the material 550. That is to say, the mechanism of the short FCG for materials 550 and 630 should be the same, accordingly, the FCG rate should have a negative correlation with the yield strength. Furthermore, this kind of relationship can be derived directly from the crack tip opening displacement (CTOD) theory.

The relationship between CTOD and FCG rate is the basis of many dislocation models for the theoretical calculation of fatigue cracking law. In general, the CTOD can be calculated by [25]:

$$\Delta CTOD \approx \frac{\Delta K^2}{2\sigma_{\mathrm{YS}} E'}, \tag{3}$$

where ΔK is the range of stress intensity factor, σ_{YS} is the yield strength and E is Young's modulus. Because the composition of the material remains unchanged, E may be considered as a constant. Therefore, the $\Delta CTOD$ of the three materials under certain ΔK should be only related to their yield strength. Considering the geometrical relationship between the striation spacing, the following relationship could be obtained [11, 25]:

$$\frac{\mathrm{d}a}{\mathrm{d}N} \propto \Delta CTOD \propto \frac{1}{\sigma_{\mathrm{YS}}}. \tag{4}$$

The prediction that $\mathrm{d}a/\mathrm{d}N \propto 1/\sigma_{\mathrm{YS}}$ is observed in both finite element simulation [26, 27] and experimental results [28, 29].

Based on the analysis and experimental results above, it is considered that the Paris coefficient C is inversely proportional to yield strength. By using the fatigue data of materials 550 and 630, the following equation can be obtained:

$$C = \frac{1.89\times10^{-7}}{\sigma_{\mathrm{YS}}}\ \mathrm{mm/cycle}. \tag{5}$$

Fig. 7 shows the experimental results and the predicted result calculated by Eq. (5). It is evident that the relationship of FCG rate and yield strength for materials 630

and 550 agrees well with the CTOD theory, while the FCG rate of material 500 is faster than the predicted value. The abnormal faster FCG rate might be traced to the different crack propagation morphology. As shown in Fig. 5, LB cracks were found in material 500, but not in materials 550 and 630. Therefore, the effect of the LB cracking on the short FCG rate must be taken into account and better be quantified.

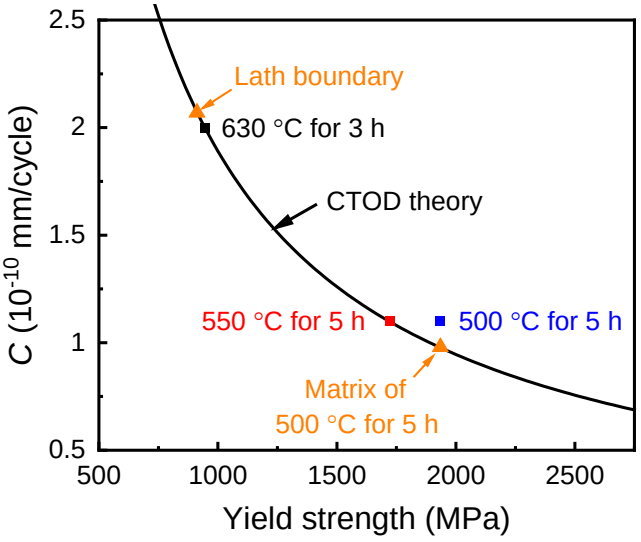

Fig. 7. The coefficient *C* in Paris law of experimental results and the predicted value calculated by CTOD theory.

4.2. Influence of the lath boundary cracking in material 500

The influence of LB cracking on FCG rate in material 500 can be attributed to two aspects. Firstly, the FCG rate of LB differed considerably from the matrix due to the difference in strength. Secondly, the orientation of LB could also affect the FCG behavior by altering the crack grow path length.

Previously, Eq. (5) shows that the coefficient *C* in Paris law is related to the yield strength. As for the yield strength, it is believed that the strengthening mechanism in the present maraging steel is precipitation strengthening, so the yield strength can be calculated by the Orowan mechanism [30, 31]:

$$\sigma_{YS} = \sigma_0 + K\frac{\ln(\frac{d}{b})}{\lambda}, \tag{6}$$

where σ_0 is the tensile yield strength of the unaged matrix, K is constant, b is the Burgers vector, d is the spherical diameters, and λ is the interparticle spacing. The size of the

precipitates d and the spacing between them λ are listed in Table 4 [7]. By fitting the data in Table 4 with Eq. (6), the two variables σ_0 and K can be obtained to be 912 MPa and 3747 MPa/m, respectively. It is believed that there should be no precipitation strengthening at the LB for the specimens under three heat treatment conditions [15]. Therefore, the strength of the LB without precipitation strengthening can be considered to be σ_0, which is 912 MPa. After that, the theoretical value of Pairs coefficient C of LB is calculated through Eq. (5) to be 2.07×10^{-10} mm/cycle as marked in Fig. 7.

Table 4. The size of precipitates and the spacing between precipitates for specimens under different ageing treatment.

Material label	Spherical Diameter, d (nm)	Interparticle spacing, λ (nm)
500	14.9	14
550	26.5	28
630	62.4	98

As for the effect of the orientation of LB on the global FCG rate, it is considered by using the integral average method in mathematics. As shown in Fig. 8, the crack growth is divided into two parts: intra-lath crack and inter-lath crack (LB crack). For a general situation shown in Fig. 8, the FCG rate could be calculated using the total distance to divide the total time. The total time consists of the intra-lath crack part and the inter-lath part. The FCG rate could be given by:

$$\frac{\mathrm{d}a}{\mathrm{d}N}=\frac{1}{\dfrac{\sin\theta}{\dfrac{\mathrm{d}a}{\mathrm{d}N}\Big|_{\text{Inter-lath}}}+\dfrac{\cos\theta}{\dfrac{\mathrm{d}a}{\mathrm{d}N}\Big|_{\text{Intra-lath}}}}, \tag{7}$$

where θ is the angle between the LB and the primary crack. Then, considering all possibilities of θ, the global average FCG rate could be obtained by:

$$\frac{\mathrm{d}a}{\mathrm{d}N}\Big|_{\text{Average}}=\frac{2}{\pi}\int_0^{\frac{\pi}{2}}\frac{1}{\dfrac{\sin\theta}{\dfrac{\mathrm{d}a}{\mathrm{d}N}\Big|_{\text{Inter-lath}}}+\dfrac{\cos\theta}{\dfrac{\mathrm{d}a}{\mathrm{d}N}\Big|_{\text{Intra-lath}}}}. \tag{8}$$

As previously mentioned, the Pairs exponent m for specimens of all three heat treatment conditions are almost equal. Therefore Eq. (8) could be simplified by replacing the $\mathrm{d}a/\mathrm{d}N$ by the Pairs coefficient C:

$$C_{\text{Average}} = \frac{2}{\pi}\int_0^{\frac{\pi}{2}} \frac{1}{\frac{\sin\theta}{C_{\text{Inter-lath}}} + \frac{\cos\theta}{C_{\text{Intra-lath}}}}, \tag{9}$$

where the $C_{\text{inter-lath}}$ and $C_{\text{intra-lath}}$ for material 500 are calculated by Eq. (5), which is 2.07×10^{-10} mm/cycle and 9.8×10^{-11} mm/cycle, respectively. It is obvious that the short FCG rate of LB is faster than that of the matrix.

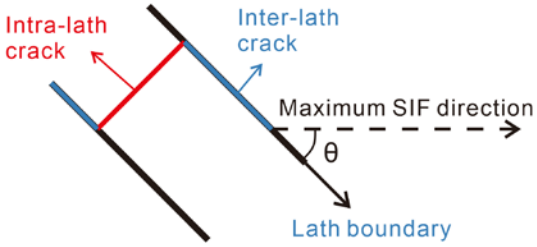

Fig. 8. Schematically illustration of the geometric relationship of the intra-lath crack and the inter-lath crack. θ refers to the angle between the maximum stress intensity factor (SIF) direction and the lath boundary.

Fig. 9 shows the experimental result, the prediction of CTOD theory, and the prediction of CTOD theory with LB cracking. It is evident that, by considering the effects of LB cracking, the prediction value is equative to the experimental one.

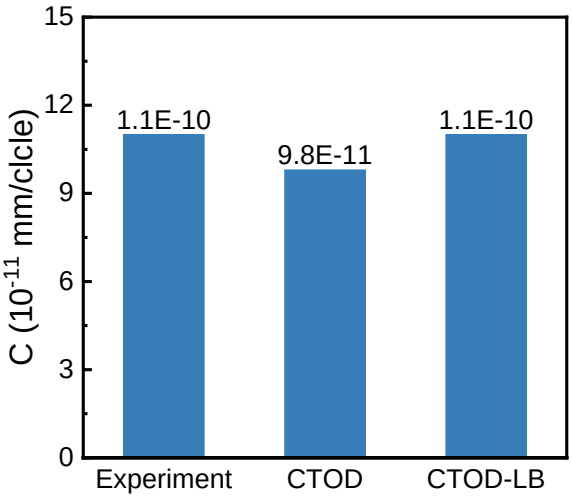

Fig. 9. The coefficient C in Paris law of material 500 measured by experiment, calculated by CTOD theory and CTOD theory with LB cracking.

4.3. Reasons for the lath boundary cracking

The analysis shows that two key factors might affect the cracking of LB: the difference in the strength between LB and intra-lath and the width of the LB. Fig. 10 shows the difference in the yield strength between LB and intra-lath. Their difference is caused by the absence of precipitate strengthening in LB. Therefore, the strength of LB is represented by the tensile yield strength σ_0 of the unaged matrix in Eq. (6). It can be seen from Fig. 10 that material 500 has the biggest difference in the strength between the LB and intra-lath. The large difference in strength will cause serious strain heterogeneity during the cyclic loading so that the material 500 has the maximum probability to crack in LB [15].

On the other hand, the width of LB can also affect the degree of strain heterogeneity in LB. Increasing the width of LB can be beneficial for the evacuation of dislocations from the interface of reverted austenite and martensite lath [32]. Besides, increasing the width of LB also rises the dislocation capacity of LB so that the LB could undertake more deformation. Fig. 11 shows the width of the LB for specimens aged at different temperatures. It is evident that material 500 has the smallest width of LB so that it has the maximum probability of cracking in LB.

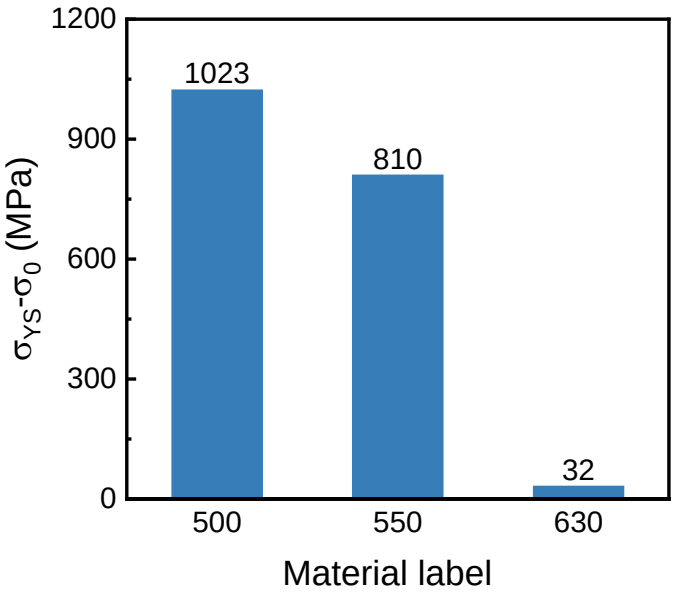

Fig. 10. The difference in the yield strength between intra-lath and inter-lath.

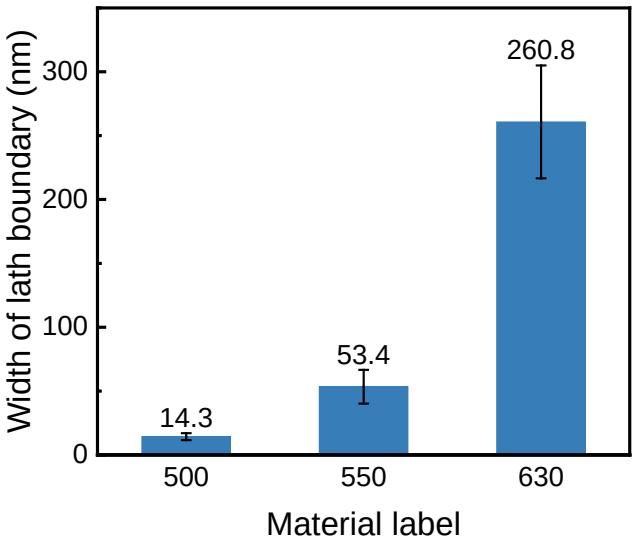

Fig. 11. Widths of the lath boundary for specimens under different ageing treatments.

4.4. Acceleration or deceleration of fatigue cracking

The results in this study show that the LB cracking in material 500 could accelerate the short FCG. As for the materials 550 and 630, the calculation results for LB cracking are shown in Fig. 12 marked by triangles. It can be seen that for the present maraging steels, the LB cracking, which is referred to as the zigzag path, could accelerate the short FCG rate when the difference in the strength between the matrix and the LB is larger than 588 MPa. The zigzag path could only decelerate the crack growth when the difference in strength between the LB and the matrix is smaller than 588 MPa.

This is because the reference objected to compare with for FCG rate is the matrix. For materials 500 and 550, their FCG rates of the matrix are relatively slow. Although the LB cracking could cause the zigzag path which could increase the crack path length, the FCG rate of LB is so fast than that of the matrix that it ends up with a faster global average FCG rate. For material 630, the FCG rate of the matrix is relatively fast so the increased crack path length due to the zigzag path may lead to a slower global average FCG rate. That might be the explanation of why there are some cases in the literature that the zigzag path could depress the fatigue crack. However, it should be noted that when the yield strength decreases, the LB cracking driven force also reduces. Therefore, the optimum short crack growth resistance would be obtained within the heat treatment range of 500 ℃ and 550 ℃.

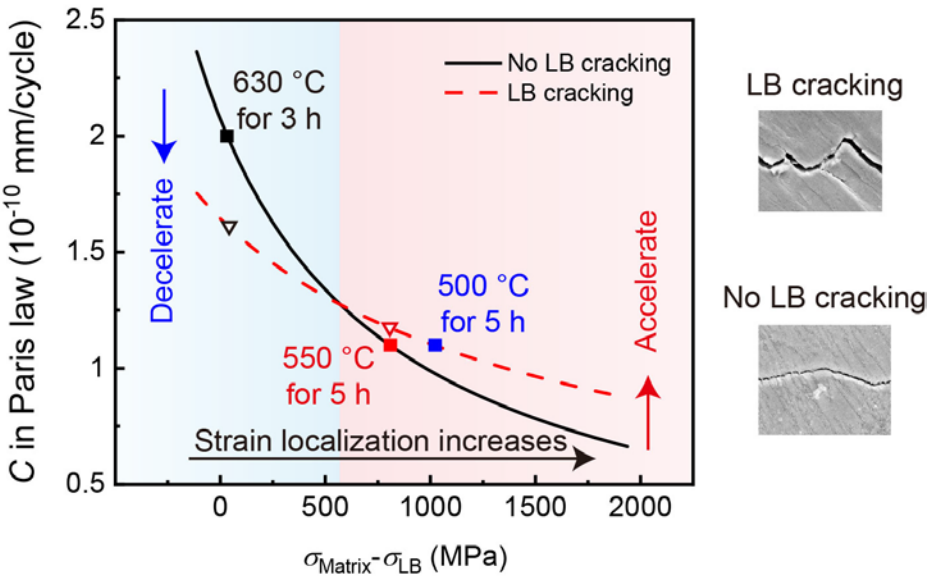

Fig. 12. The influence of the LB cracking on the short fatigue crack growth rate.

5. Conclusions

Studies focusing on short FCG behaviors of 18Ni maraging steel aged at 500 ℃ for 5 h, 550 ℃ for 5 h, and 630 ℃ for 3 h were conducted. Based on the experimental results and analysis, the following conclusions can be drawn:

(1) The short FCG rate of the 18Ni maraging steel could be obtained by analyzing the residual life of multiple specimens containing the different lengths of initial cracks and it can be described by Pairs law.

(2) The Pairs exponent *m* is not affected by the ageing treatment, while the Paris coefficient *C* is related to yield strength in 18Ni maraging steels. Increasing the yield strength can decrease the FCG rate. However, as the yield strength further increases the LB cracking occurs, which would accelerate the FCG rate.

(3) By dividing the fatigue cracks in material 500 into the intra- and inter-lath crack, the global FCG rate can be calculated by using the integral average method.

(4) The LB cracking in material 500 could be traced to the largest difference in strength between LB and intra-lath and the smallest width of the LB.

(5) For the failures in the regime 1000 - 10000, the optimum crack growth resistance can be obtained in the high-strength region where the cracking mode changes. In the present study, it is in the heat treatment range from 500 ℃ to 550 ℃ for 5 h.

(6) The zigzag crack growth path is not always beneficial for the higher fatigue cracking resistance. In a multi-phase material, when the difference of strength between the phases is large enough, the weaker phase could lead to a zigzag path and a faster FCG rate simultaneously. Therefore, it is too absolute to equate the appearance of zigzag path and the optimal crack growth resistance in the material design.

Declaration of competing interest

The authors declare that they have no known competing financial interests or personal relationships that could have appeared to influence the work reported in this paper.

CRediT Author Statement

Zikuang Xu: Conceptualization, Formal analysis, Investigation, Data curation, Writing – original draft. **Bin Wang:** Resources, Writing – review & editing. **Peng Zhang:** Conceptualization, Methodology, Supervision, Writing – review & editing. **Zhefeng Zhang:** Supervision, Writing – review & editing.

Acknowledgments

This work was financially supported by the National Natural Science Foundation of China (NSFC) under grant Nos. 51771208, U1664253, 52001310, the Strategic Priority Research Program of the Chinese Academy of Sciences under grant Nos. XDB22020202, XDC04040502, the LiaoNing Revitalization Talents Program under grant No. XLYC1808027, Youth Innovation Promotion Association CAS under grant No. 2018226 and China Postdoctoral Science Foundation under grant No. 2020M670810.

Data availability

Data will be made available on request.

References

[1] V.K. Vasudevan, S.J. Kim, C.M. Wayman, Precipitation reactions and strengthening behavior in 18 Wt Pct nickel maraging steels, Metall. Trans. A 21(10) (1990) 2655-2668.

[2] M. Shmulevitsh, L. Meshi, M. Pinkas, R.Z. Shneck, Elastic consideration of the precipitation in model alloys of maraging steels: Theory and experimental validation, J. Mater. Sci. 50(14) (2015) 4970-4979.

[3] W. Wang, W. Yan, Q.Q. Duan, Y.Y. Shan, Z.F. Zhang, K. Yang, Study on fatigue property of a new 2.8GPa grade maraging steel, Mater. Sci. Eng. A 527(13-14) (2010) 3057-3063.

[4] W.M. Garrison, Ultrahigh-strength steels for aerospace applications, JOM 42(5) (1990) 20-24.

[5] Y. Tomita, Development of fracture toughness of ultrahigh strength low alloy steels for aircraft and aerospace applications, Mater. Sci. Technol. 7(6) (1991) 481-489.

[6] J.W. Morris Jr, Making steel strong and cheap, Nat. Mater. 16 (2017) 787.

[7] B. Wang, P. Zhang, Q.Q. Duan, Z.J. Zhang, H.J. Yang, X.W. Li, Z.F. Zhang, Optimizing the fatigue strength of 18Ni maraging steel through ageing treatment, Mater. Sci. Eng. A 707(Supplement C) (2017) 674-688.

[8] S. Suresh, R.O. Ritchie, Propagation of short fatigue cracks, Int. Met. Rev. 29(6) (1984) 445-76.

[9] H. Li, M. Koyama, T. Sawaguchi, K. Tsuzaki, H. Noguchi, Importance of crack-propagation-induced ε-martensite in strain-controlled low-cycle fatigue of high-Mn austenitic steel, Philos. Mag. Lett. 95(6) (2015) 303-311.

[10] Y.B. Ju, M. Koyama, T. Sawaguchi, K. Tsuzaki, H. Noguchi, In situ microscopic observations of low-cycle fatigue-crack propagation in high-Mn austenitic alloys with deformation-induced ε-martensitic transformation, Acta Mater. 112 (2016) 326-336.

[11] T. Leitner, A. Hohenwarter, W. Ochensberger, R. Pippan, Fatigue crack growth anisotropy in ultrafine-grained iron, Acta Mater. 126 (2017) 154-165.

[12] F. Briffod, A. Bleuset, T. Shiraiwa, M. Enoki, Effect of crystallographic orientation and geometrical compatibility on fatigue crack initiation and propagation in rolled Ti-6Al-4V alloy, Acta Mater. 177 (2019) 56-67.

[13] K. Wang, R. Bao, B. Jiang, Y. Wu, D. Liu, C. Yan, Effect of primary α phase on the fatigue crack path of laser melting deposited Ti–5Al–5Mo–5V–1Cr–1Fe near β titanium alloy, Int. J. Fatigue 116 (2018) 535-542.

[14] B. Alfredsson, M. Öberg, J. Lai, Propagation of physically short cracks in a bainitic high strength bearing steel due to fatigue load, Int. J. Fatigue 90 (2016) 166-180.

[15] Z.K. Xu, B. Wang, P. Zhang, Z.F. Zhang, A fast evaluation method for fatigue strength of maraging steel: The minimum strength principle, Mater. Sci. Eng. A 789 (2020) 139659.

[16] P.P. Sinha, D. Sivakumar, N.S. Babu, K.T. Tharian, A. Natarajan, Austenite reversion in 18 Ni Co-free maraging steel, Steel Res. 66(11) (1995) 490-494.

[17] P.P. Sinha, K.T. Tharian, K. Sreekumar, K.V. Nagarajan, D.S. Sarma, Effect of aging on microstructure and mechanical properties of cobalt free 18%Ni (250 grade) maraging steel, Mater. Sci. Technol. 14(1) (1998) 1-9.

[18] K. Li, B. Yu, R.D.K. Misra, G. Han, S. Liu, C.J. Shang, Strengthening of cobalt-free 19Ni3Mo1.5Ti maraging steel through high-density and low lattice misfit nanoscale precipitates, Mater. Sci. Eng. A 715 (2018) 174-185.

[19] K. Li, L. Wei, B. An, B. Yu, R.D.K. Misra, Aging phenomenon in low lattice-misfit cobalt-free maraging steel: Microstructural evolution and strengthening behavior, Mater. Sci. Eng. A 739 (2019) 445-454.

[20] F. Qian, J. Sharp, W.M. Rainforth, Microstructural evolution of Mn-based maraging steels and their influences on mechanical properties, Mater. Sci. Eng. A 674 (2016) 286-298.

[21] H. Leitner, M. Schober, R. Schnitzer, S. Zinner, Strengthening behavior of Fe–Cr–Ni–Al–(Ti) maraging steels, Mater. Sci. Eng. A 528(15) (2011) 5264-5270.

[22] M. Niu, G. Zhou, W. Wang, M.B. Shahzad, Y. Shan, K. Yang, Precipitate evolution

and strengthening behavior during aging process in a 2.5 GPa grade maraging steel, Acta Mater. 179 (2019) 296-307.

[23] T. Connolley, P.A.S. Reed, M.J. Starink, Short crack initiation and growth at 600°C in notched specimens of Inconel718, Mater. Sci. Eng. A 340(1-2) (2003) 139-154.

[24] H.F. Li, S.G. Wang, P. Zhang, R.T. Qu, Z.F. Zhang, Crack propagation mechanisms of AISI 4340 steels with different strength and toughness, Mater. Sci. Eng. A 729 (2018) 130-140.

[25] S. Suresh, Fatigue of Materials, Cambridge University Press, Cambridge, 1998.

[26] F.V. Antunes, R. Branco, P.A. Prates, L. Borrego, Fatigue crack growth modelling based on CTOD for the 7050-T6 alloy, Fatigue Fract. Eng. Mater. Struct. 40(8) (2017) 1309-1320.

[27] F.V. Antunes, S.M. Rodrigues, R. Branco, D. Camas, A numerical analysis of CTOD in constant amplitude fatigue crack growth, Theor. Appl. Fract. Mech. 85 (2016) 45-55.

[28] J.M. Vasco-Olmo, F.A. Díaz, F.V. Antunes, M.N. James, Characterisation of fatigue crack growth using digital image correlation measurements of plastic CTOD, Theor. Appl. Fract. Mech. 101 (2019) 332-341.

[29] W. Guo, C.H. Wang, L.R.F. Rose, The influence of cross-sectional thickness on fatigue crack growth, Fatigue Fract. Eng. Mater. Struct. 22(5) (1999) 437-444.

[30] U.K. Viswanathan, G.K. Dey, M.K. Asundi, Precipitation hardening in 350 grade maraging steel, Metall. Trans. A 24(11) (1993) 2429-2442.

[31] E.V. Pereloma, A. Shekhter, M.K. Miller, S.P. Ringer, Ageing behaviour of an Fe–20Ni–1.8Mn–1.6Ti–0.59Al (wt%) maraging alloy: Clustering, precipitation and hardening, Acta Mater. 52(19) (2004) 5589-5602.

[32] B.S. Gong, Z.J. Liu, Y.L. Wang, Z.J. Zhang, P. Zhang, H.C. Jiang, L.J. Rong, Z.F. Zhang, Improving the fatigue strength of A7N01 aluminum alloy by adjusting Si content, Mater. Sci. Eng. A 742 (2019) 15-22.